

Direct numerical reconstruction of conductivities in three dimensions

Jutta Bikowski¹, Kim Knudsen², Jennifer Mueller³

¹ Agrosphere, ICG-4, Forschungszentrum Jülich, Jülich, Germany

² Department of Mathematics, Technical University of Denmark, Kgs. Lyngby, Denmark

³ Department of Mathematics, Colorado State University, Fort Collins

E-mail: jubi305@gmail.com, k.knudsen@mat.dtu.dk, mueller@math.colostate.edu

AMS classification scheme numbers: 35R30, 65N21

Abstract. A direct three dimensional EIT reconstruction algorithm based on complex geometrical optics solutions and a nonlinear scattering transform is presented and implemented for spherically symmetric conductivity distributions. The scattering transform is computed both with a Born approximation and from the forward problem for purposes of comparison. Reconstructions are computed for several test problems. A connection to Calderón's linear reconstruction algorithm is established, and reconstructions using both methods are compared.

1. Introduction

The reconstruction of conductivity distributions in two or three dimensions from measurements of the current density-to-voltage map is known as electrical impedance tomography, or EIT, and has applications in medical imaging, nondestructive testing, and geophysics. For the 3-D bounded domain considered here, medical applications include head imaging and the detection of breast tumors. See, for example, [Hol05] for a survey of clinical applications of EIT. In this work, we consider a bounded domain in \mathbf{R}^3 and present a direct reconstruction algorithm and its numerical implementation on the unit sphere. The theoretical foundation of the method dates back more than 20 years to a series of papers by Sylvester-Uhlmann [SU87], Novikov [Nov88], Nachman-Sylvester-Uhlmann [NSU88] and Nachman [Nac88]. The algorithm makes use of complex geometrical optics (CGO) solutions to the Schrödinger equation and uses the inverse scattering method. This is described in detail in section 2 of this paper.

The inverse conductivity problem was first formulated mathematically by Calderón [Cal80] as follows. Let $\Omega \subset \mathbf{R}^n, n \geq 3$ be a simply connected, bounded domain with smooth boundary $\partial\Omega$, and let $\gamma \in L^\infty(\Omega)$ denote the conductivity distribution. Assume there exists $C > 0$ such that for $x \in \Omega$, $C^{-1} \leq \gamma(x) \leq C$. The electric potential u arising from the application of a known voltage to the boundary of Ω is modeled by the generalized Laplace equation with Dirichlet boundary condition

$$\nabla \cdot \gamma \nabla u = 0 \text{ in } \Omega, \quad u = f \text{ on } \partial\Omega. \quad (1)$$

The Dirichlet-to-Neumann map Λ_γ is defined by

$$\Lambda_\gamma f = \gamma \frac{\partial u}{\partial \nu} \Big|_{\partial\Omega}. \quad (2)$$

Thus Λ_γ represents static electrical boundary measurements: it maps an applied voltage distribution on the boundary to the resulting current flux through the boundary. Calderón [Cal80] posed the question of whether the conductivity γ is uniquely determined by the Dirichlet-to-Neumann map, and if so, how to reconstruct the conductivity. He gave an affirmative answer to the uniqueness question for the linearized problem and gave a reconstruction algorithm for that case. His algorithm is described in section 2.3 of this paper.

The uniqueness question for $\gamma \in L^\infty(\Omega)$ is still open in \mathbf{R}^3 , but has been solved recently by Astala and Päiväranta [AP06b] for a bounded domain in \mathbf{R}^2 , sharpening the previous results due to Nachman [Nac96] in which $\gamma \in W^{2,p}(\Omega)$, $p > 1$, and Brown and Uhlmann [BU97] in which $\gamma \in W^{1,p}(\Omega)$, $p > 2$. In three dimensions the uniqueness problem was solved for smooth conductivities in [SU87]. At the time of this publication, in \mathbf{R}^3 the uniqueness results with lowest regularity are [BT03] with $\gamma \in W^{3/2,p}(\Omega)$, $p > 2n$ and [PPU03] with $\gamma \in W^{3/2,\infty}(\Omega)$.

Most existing 3-D EIT reconstruction algorithms are linear or iterative, minimizing a functional that describes the nearness of the predicted voltages to the measured data in a given norm with one or more regularization terms. In contrast, the algorithm presented here is direct and fully nonlinear. It is similar to the 2-D D-bar

algorithms based on the works [Nac96] and [BU97], which were first implemented in [SMI00, SMI01, Knu03, MS03]. In these initial works the Born approximation to the CGO solutions is used in the computation of the scattering transform. It was used successfully on experimental tank data in, for example, [IMNS04, EM09] and human chest data in [IMNS06, DM10]. This inspired the approach in section 2.2 of this paper in which the Born approximation is used in the 3-D direct algorithm. For further reading on 2-D D-bar algorithms, the reader is referred to [KLMS07] in which the application to discontinuous conductivity distributions is specifically addressed, and [KLMS09] in which a rigorous regularization framework is established using the full scattering transform. Calderón's method has also recently been used for the reconstruction from experimental data in both 2-D [BM08] and 3-D [BTJIS08].

In this work, we assume the conductivity $\gamma \in C^2(\overline{\Omega})$, we take Ω to be the unit sphere in \mathbf{R}^3 , and assume $\gamma = 1$ near $\partial\Omega$. The smoothness assumption on γ is necessary, but the other assumptions are made mainly for simplicity in the numerical computations. We stress in particular that the theory is valid in more complex geometries. The study of the effects of noise in the data is not in the scope of this paper, but rather is left for future work.

The outline of the paper is as follows. In section 2.2 we describe a direct reconstruction algorithm with a linearizing assumption tantamount to a Born approximation. That approach is referred to as the \mathbf{t}^{exp} approach, consistent with the notation used in the 2-D D-bar algorithms. An explicit connection to the linearized method of Calderón is established in section 2.3. The reconstruction of the conductivity in the 2-D D-bar method described in the works above is achieved by taking a small frequency limit in a D-bar equation for the CGO solutions to directly obtain $\gamma(x)$. In contrast, here we have to take a high complex frequency limit. A D-bar equation for the 3-D problem is utilized in [CKS06], resulting in a promising, but more complicated approach than the one studied here. The numerical implementation of that approach is left for future work. In section 3 we consider the case of spherically symmetric conductivities and show symmetry properties in the scattering transform. We also show how the Dirichlet-to-Neumann map can be represented and approximated in that case. Details on the numerical implementation are found in section 4. Numerical examples are found in section 5.

2. The reconstruction methods

In this section we describe the theoretical reconstruction method, the \mathbf{t}^{exp} approach, and the relationship to Calderón's linearized method.

2.1. The nonlinear reconstruction method

The method was developed in [SU87, Nov88, NSU88, Nac88]; here we provide a brief outline. The reader is referred to [Nac88] for rigorous proofs. The equations closely

parallel those of the 2-D problem (note that [Nac88] precedes that work), and so readers familiar with that case will recognize the notation and functions involved.

The initial step is to transform the conductivity equation into a Schrödinger equation. Indeed, if u satisfies (1) then $v = \gamma^{1/2}u$ satisfies

$$(-\Delta + q)v = 0 \text{ in } \Omega \quad \text{with} \quad q = \frac{\Delta\gamma^{1/2}}{\gamma^{1/2}}. \quad (3)$$

Note that $q = 0$ near $\partial\Omega$. The Dirichlet-to-Neumann map for equation (3) is defined by

$$\Lambda_q f = \frac{\partial v}{\partial \nu} \Big|_{\partial\Omega},$$

where now v satisfies (3) with $v|_{\partial\Omega} = f$. In general the maps Λ_γ and Λ_q are related by

$$\Lambda_q = \gamma^{-1/2} \left(\Lambda_\gamma + \frac{1}{2} \frac{\partial \gamma}{\partial \nu} \right) \gamma^{-1/2}. \quad (4)$$

The assumption that $\gamma = 1$ in a neighborhood of $\partial\Omega$ simplifies (4) to $\Lambda_q = \Lambda_\gamma$.

To define the CGO solutions, introduce a complex frequency parameter $\zeta \in \mathbb{C}^3$ and define the set

$$\mathcal{V} = \{\mathbb{C}^3 \setminus \{0\} : \zeta \cdot \zeta = 0\}. \quad (5)$$

Then $e^{ix \cdot \zeta}$ is harmonic in \mathbf{R}^3 if and only if $\zeta \in \mathcal{V}$. For $\xi \in \mathbf{R}^3$, introduce the subset of \mathcal{V} given by

$$\mathcal{V}_\xi = \{\zeta \in \mathcal{V} : (\xi + \zeta)^2 = 0\}. \quad (6)$$

Note that $\zeta \cdot \zeta = (\xi + \zeta)^2 = 0$ gives an explicit characterization of \mathcal{V}_ξ in terms of an auxiliary vector $\xi^\perp \in \mathbf{R}^3$ with $\xi^\perp \cdot \xi = 0$. Indeed suppose $\zeta_R, \zeta_I \in \mathbf{R}^3$. Then $\zeta = \zeta_R + i\zeta_I \in \mathcal{V}_\xi$ if and only if

$$\begin{aligned} \zeta_R &= -\xi/2 + \xi^\perp, \\ \zeta_I \cdot \xi &= \zeta_I \cdot \xi^\perp = 0, \quad |\zeta_I| = |\zeta_R|. \end{aligned} \quad (7)$$

Since $q = 0$ in a neighborhood of $\partial\Omega$, one can extend $q = 0$ into $\mathbf{R}^3 \setminus \overline{\Omega}$. The CGO solutions $\psi(x, \zeta)$ to the Schrödinger equation solve

$$(-\Delta + q(x))\psi(x, \zeta) = 0, \quad x \in \mathbf{R}^3, \quad \zeta \in \mathcal{V}, \quad (8)$$

and behave like $e^{ix \cdot \zeta}$ for $|\zeta|$ large. More precisely, define

$$\mu(x, \zeta) = \psi(x, \zeta) e^{-ix \cdot \zeta}.$$

Then $\mu - 1$ approaches zero in a certain sense as either $|x|$ or $|\zeta|$ tends to infinity, see [SU87, Nac88]. Note that $\psi(x, \zeta)$ grows exponentially for $x \cdot \text{Im}\zeta < 0$. The function μ satisfies

$$(-\Delta - 2i\zeta \cdot \nabla + q)\mu(x, \zeta) = 0 \text{ in } \mathbf{R}^3. \quad (9)$$

Denote by G_ζ the Faddeev Green's function defined by

$$G_\zeta(x) = e^{ix \cdot \zeta} g_\zeta(x), \quad \text{where} \quad g_\zeta(x) = \frac{1}{(2\pi)^3} \int_{\mathbf{R}^3} \frac{e^{ix \cdot \xi}}{|\xi|^2 + 2\xi \cdot \zeta} d\xi, \quad (10)$$

where the integral is understood in the sense of the Fourier transform defined on the space of tempered distributions. The functions G_ζ, g_ζ are fundamental solutions of the Laplace equation and conjugate Laplace equation respectively, i.e.

$$\Delta_\zeta g_\zeta = -\delta_0 \quad \text{and} \quad \Delta G_\zeta = -\delta_0. \quad (11)$$

Then (9) is equivalent to the Faddeev-Lippmann-Schwinger equation

$$(I + g_\zeta * (q \cdot))\mu = 1 \text{ in } \mathbf{R}^3. \quad (12)$$

Estimates for the operator $g_\zeta*$ for large ζ ([SU87]) and small ζ ([CKS06]) give the existence and uniqueness of μ (and therefore ψ) for any sufficiently large or small $\zeta \in \mathcal{V}$.

The key intermediate object in the reconstruction method is the so-called non-physical scattering transform of the potential q defined for $\xi \in \mathbf{R}^3$ and sufficiently large or small $\zeta \in \mathcal{V}$ by

$$\mathbf{t}(\xi, \zeta) = \int_{\Omega} e^{-ix \cdot (\xi + \zeta)} \psi(x, \zeta) q(x) dx. \quad (13)$$

Integrating by parts and assuming that $\zeta \in \mathcal{V}_\xi$ we find that

$$\mathbf{t}(\xi, \zeta) = \int_{\partial\Omega} e^{-ix \cdot (\xi + \zeta)} (\Lambda_q - \Lambda_0) \psi(x, \zeta) d\sigma(x). \quad (14)$$

Thus we require $\psi|_{\partial\Omega}$ in order to compute the scattering transform from the Dirichlet-to-Neumann map. It turns out that $\psi|_{\partial\Omega}$ satisfies a uniquely solvable Fredholm integral equation of the second kind on $\partial\Omega$ [Nov88, Nac88], namely,

$$\psi(x, \zeta) + \int_{\partial\Omega} G_\zeta(x - \tilde{x}) (\Lambda_q - \Lambda_0) \psi(\tilde{x}, \zeta) d\sigma(\tilde{x}) = e^{ix \cdot \zeta}, \quad x \in \partial\Omega. \quad (15)$$

Note from (13) and the fact that $\psi \sim e^{i\zeta \cdot x}$ that from the scattering transform one can compute the Fourier transform \hat{q} of the potential by taking the large frequency limit

$$\lim_{|\zeta| \rightarrow \infty} \mathbf{t}(\xi, \zeta) = \hat{q}(\xi). \quad (16)$$

Summary of the reconstruction method:

- (i) Solve the boundary integral equation (15) for $\psi|_{\partial\Omega}$.
- (ii) Compute $\mathbf{t}(\xi, \zeta)$ for $\xi \in \mathbf{R}^3, \zeta \in \mathcal{V}_\xi$ by (14).
- (iii) Compute $\hat{q}(\xi)$ from (16).
- (iv) Compute q by inverting the Fourier transform.
- (v) Compute γ by solving $-\Delta\sqrt{\gamma} + q\sqrt{\gamma} = 0$ in Ω , $\sqrt{\gamma}|_{\partial\Omega} = 1$.

We stress that the ill-posedness of the inverse problem is in this algorithm isolated in the first step.

2.2. The reconstruction method using \mathbf{t}^{exp}

Inspired by the \mathbf{t}^{exp} approximation in the 2-D D-bar method, an analogous approach can be taken in 3-D. Approximating $\psi(x, \zeta)$ on the boundary by its asymptotic behavior $e^{ix \cdot \zeta}$ eliminates the need for the ill-posed first step. We define for $\xi \in \mathbf{R}^3, \zeta \in \mathcal{V}_\xi$

$$\mathbf{t}^{\text{exp}}(\xi, \zeta) = \int_{\partial\Omega} e^{-ix \cdot (\xi + \zeta)} (\Lambda_q - \Lambda_0) e^{ix \cdot \zeta} d\sigma(x). \quad (17)$$

This approximation is tantamount to a linearization of the first step in the reconstruction algorithm above around $\gamma = 1$. Using \mathbf{t}^{exp} for \mathbf{t} in (16) gives the following simple reconstruction algorithm:

- (i) Compute $\mathbf{t}^{\text{exp}}(\xi, \zeta)$ for $\xi \in \mathbf{R}^3$, $\zeta \in \mathcal{V}_\xi$ by (17).
- (ii) Compute

$$\widehat{q^{\text{exp}}}(\xi) = \lim_{|\zeta| \rightarrow \infty} \mathbf{t}^{\text{exp}}(\xi, \zeta) \quad (18)$$

and then q^{exp} by inverting the Fourier transform.

- (iii) Compute γ^{exp} by solving $-\Delta \sqrt{\gamma^{\text{exp}}} + q^{\text{exp}} \sqrt{\gamma^{\text{exp}}} = 0$ in Ω $\sqrt{\gamma^{\text{exp}}}|_{\partial\Omega} = 1$.

It is not guaranteed from the theory that the limit in (18) is well-defined. In our numerical simulations we will compute $\mathbf{t}^{\text{exp}}(\xi, \zeta)$ for a fixed but large value of ζ . This will numerically define $\widehat{q^{\text{exp}}}(\xi)$.

2.3. Calderon's linearized reconstruction method

Several properties of \mathbf{t}^{exp} can be established from an analysis comparing this approach to that of Calderón. In [KLMS07] a connection was established between the 2-D D-bar method based on the global uniqueness proof by Nachman [Nac96] and Calderón's linearized reconstruction method.

Define a function $u^{\text{exp}}(x, \zeta)$ as the unique solution to the boundary value problem

$$\begin{aligned} \nabla \cdot \gamma \nabla u^{\text{exp}}(x, \zeta) &= 0, \quad x \in \Omega, \quad \zeta \in \mathbb{C}^3 \\ u^{\text{exp}}|_{\partial\Omega} &= e^{ix \cdot \zeta}. \end{aligned}$$

Integration by parts in equation (17) results in a formula for \mathbf{t}^{exp} defined in terms of γ in the interior

$$\mathbf{t}^{\text{exp}}(\xi, \zeta) = \int_{\Omega} (\gamma - 1) \nabla u^{\text{exp}}(x, \zeta) \cdot \nabla e^{-ix \cdot (\xi + \zeta)} dx. \quad (19)$$

Write $u^{\text{exp}} = e^{ix \cdot \zeta} + \delta u$ for $\delta u \in H_0^1(\Omega)$. Then δu satisfies

$$\nabla \cdot (\gamma \nabla \delta u) = -\nabla \cdot ((\gamma - 1) \nabla e^{ix \cdot \zeta}), \quad (20)$$

and one can estimate

$$\|\delta u\|_{H^1(\Omega)} \leq C \|(\gamma - 1) \nabla e^{ix \cdot \zeta}\|_{L^2(\Omega)} \leq |\zeta| \|\gamma - 1\|_{L^\infty(\Omega)} e^{|\zeta|R}, \quad (21)$$

where R is the radius of the smallest ball containing Ω . From (19) we then get

$$\begin{aligned} \mathbf{t}^{\text{exp}}(\xi, \zeta) &= \int_{\Omega} (\gamma - 1) \nabla (e^{ix \cdot \zeta} + \delta u) \cdot \nabla e^{-ix \cdot (\xi + \zeta)} dx \\ &= \int_{\Omega} (\gamma - 1) \nabla e^{ix \cdot \zeta} \cdot \nabla e^{-ix \cdot (\xi + \zeta)} dx + R(\xi, \zeta) \\ &= (\xi \cdot \zeta) \int_{\Omega} (\gamma - 1) e^{-ix \cdot \xi} dx + R(\xi, \zeta), \end{aligned}$$

where the remainder term

$$R(\xi, \zeta) = \int_{\Omega} (\gamma - 1) \nabla \delta u \cdot \nabla e^{-ix \cdot (\xi + \zeta)} dx.$$

Since $(\xi + \zeta)^2 = \zeta^2 = 0$ we have $-\xi^2 = 2\xi \cdot \zeta$ and hence

$$\mathbf{t}^{\text{exp}}(\xi, \zeta) = -\frac{|\xi|^2}{2}(\widehat{\gamma - 1})(\xi) + R(\xi, \zeta). \quad (22)$$

The remainder is $\mathcal{O}(|\zeta|)$ for ζ small, which can be seen from (21). This fact suggests that we use the minimal $\zeta \in \mathcal{V}_\xi$, that is

$$\zeta_\xi = -\frac{\xi}{2} + i\zeta_I, \quad \text{with } \zeta_I \cdot \xi = 0, \quad |\zeta_I| = \frac{|\xi|}{2}.$$

Moreover, with this particular choice we can divide in (22) by $|\xi|^2$ as the following proposition shows.

Proposition 2.1. *Suppose $\gamma \in L^\infty(\Omega)$. Then*

$$|\mathbf{t}^{\text{exp}}(\xi, \zeta_\xi)| = \mathcal{O}(|\xi|^2)$$

for small $|\xi|$.

Proof. Note that $|\zeta_\xi|^2 = |\xi|^2/2$. Since Λ_γ maps constant functions to zero and has its range inside the space of mean free functions in $H^{-1/2}(\partial\Omega)$, we have that for small $|\xi|$

$$\begin{aligned} |\mathbf{t}^{\text{exp}}(\xi, \zeta_\xi)| &= \left| \int_{\partial\Omega} (e^{-ix \cdot (\xi + \zeta_\xi)} - 1)(\Lambda_\gamma - \Lambda_1)(e^{ix \cdot \zeta_\xi} - 1) d\sigma(x) \right| \\ &\leq C|\xi + \zeta_\xi||\zeta_\xi|, \end{aligned}$$

and hence the particular form of ζ_ξ gives the conclusion. \square

With the particular choice $\zeta = \zeta_\xi$ in (22) we now neglect the term $R(\xi, \zeta_\xi)$ and divide by $-|\xi|^2$, which gives

$$-2 \frac{\mathbf{t}^{\text{exp}}(\xi, \zeta_\xi)}{|\xi|^2} \approx (\widehat{\gamma - 1})(\xi).$$

Introduce $\chi_B(\xi)$, the characteristic function on the ball $|\xi| < B$. With this function we remove high frequencies and invert the Fourier transform. This results in a linear reconstruction algorithm

$$\gamma^{\text{app}}(x) = 1 - \frac{2}{(2\pi)^3} \int_{\mathbf{R}^3} \frac{\mathbf{t}^{\text{exp}}(\xi, \zeta_\xi)}{|\xi|^2} e^{ix \cdot \xi} \chi_B(\xi) d\xi. \quad (23)$$

This formula is equivalent to the second inversion formula obtained by Calderón [Cal80, p. 72].

In summary the linear reconstruction algorithm consists of two steps:

- (i) Compute $\mathbf{t}^{\text{exp}}(\xi, \zeta_\xi)$ by (17).
- (ii) Compute the reconstruction by (23).

This method is truly a linearization of the nonlinear reconstruction method outlined in section 2.1. As explained above \mathbf{t}^{exp} is a linearization of the first step on page 5. Moreover, the computation of the quantity

$$1 - \frac{1}{(2\pi)^3} \int_{\mathbf{R}^3} \frac{\mathbf{t}^{\text{exp}}(\xi, \zeta_\xi)}{|\xi|^2} e^{ix \cdot \xi} \chi_B(\xi) d\xi$$

linearizes the step $\hat{q} \mapsto \sqrt{\hat{q}}$. Finally, linearizing the square function gives (23).

3. The case of a spherically symmetric conductivity

As a test problem it is of special interest to consider spherically symmetric conductivities in the unit sphere. In this case the scattering transform has certain symmetry properties described below. Moreover, the Dirichlet-to-Neumann map is described explicitly in terms of eigenvalues and eigenfunctions, which in this case are the spherical harmonics. These properties will be derived in this section.

3.1. Symmetry in the scattering transform

The Fourier transform of a spherically symmetric function is spherically symmetric itself. For the scattering transforms \mathbf{t} and \mathbf{t}^{exp} we have similar properties. In the following we will tacitly assume that ζ is either small or large such that $\mathbf{t}(\xi, \zeta)$ is well-defined.

Proposition 3.1. *Let $R \in SO(2)$ be arbitrary, and suppose $q(x) = q(Rx)$ for $x \in \Omega$. Then*

$$\mathbf{t}(\xi, \zeta) = \mathbf{t}(R\xi, R\zeta), \quad \mathbf{t}^{\text{exp}}(\xi, \zeta) = \mathbf{t}^{\text{exp}}(R\xi, R\zeta) \quad (24)$$

In particular,

$$\mathbf{t}(\xi, \zeta_1) = \mathbf{t}(\xi, \zeta_2), \quad \mathbf{t}^{\text{exp}}(\xi, \zeta_1) = \mathbf{t}^{\text{exp}}(\xi, \zeta_2) \quad (25)$$

for all $\zeta_1, \zeta_2 \in \mathcal{V}_\xi$.

Proof. We will prove the result for \mathbf{t} only; for \mathbf{t}^{exp} the reasoning is similar. Let $\mathbf{R} \in SO(2)$. By the uniqueness of the CGO solutions, the rotational invariance of the Laplace operator, and the symmetry in q we have $\psi(x, \zeta) = \psi(Rx, R\zeta)$. Consider the integral (13) and make the change of variables $R^T y = x$:

$$\begin{aligned} \mathbf{t}(\xi, \zeta) &= \int_{\Omega} e^{-ix \cdot (\xi + \zeta)} \psi(x, \zeta) q(x) dx \\ &= \int_{R\Omega} e^{-iR^T y \cdot (\xi + \zeta)} \psi(R^T y, \zeta) q(R^T y) d(R^T y) \\ &= \int_{\Omega} e^{-iy \cdot R(\xi + \zeta)} \psi(y, R\zeta) q(y) dy \\ &= \mathbf{t}(R\xi, R\zeta). \end{aligned}$$

To prove (25) fix $\xi \in \mathbf{R}^3$ and take $\zeta_1, \zeta_2 \in \mathcal{V}_\xi$ with $|\zeta_1| = |\zeta_2|$. Then

$$\begin{aligned} \zeta_j &= \text{Re}(\zeta_j) + i\text{Im}(\zeta_j), \quad \text{Re}(\zeta_j) = -\frac{\xi}{2} + \xi_j^\perp \xi_j^\perp \cdot \xi = 0, \\ \text{Im}(\zeta_j) \cdot \xi &= \text{Im}(\zeta_j) \cdot \xi^\perp = 0. \end{aligned}$$

Define a linear transformation R by $R\xi = \xi$, $R\xi_1^\perp = \xi_2^\perp$, $R(\xi \times \xi_1^\perp) = \xi \times \xi_2^\perp$. As a consequence $R \in SO(2)$ and (25) follows from (24). \square

The Fourier transform of a real and even function is real itself. For the scattering transform we have the following equivalent property:

Proposition 3.2. *Suppose $q(x)$ is real and even. Then for $\xi \in \mathbf{R}^3$, $\zeta \in \mathcal{V}_\xi$*

$$\overline{\mathbf{t}(\xi, \zeta)} = \mathbf{t}(\xi, \bar{\zeta}), \quad \overline{\mathbf{t}^{exp}(\xi, \zeta)} = \mathbf{t}^{exp}(\xi, \bar{\zeta}). \quad (26)$$

Proof. We will again only show the properties for \mathbf{t} . From the uniqueness of the CGO solutions it follows that if q is even then $\mu(-x, \zeta) = \mu(x, -\zeta)$. Moreover, if q is real, then $\overline{\mu(x, \zeta)} = \mu(x, -\bar{\zeta})$. Hence, if q is both even and real then

$$\begin{aligned} \overline{\mathbf{t}(\xi, \zeta)} &= \int_{\Omega} e^{ix \cdot \xi} \overline{q(x) \mu(x, \zeta)} dx = \int_{\Omega} e^{-i(-x) \cdot \xi} q(x) \mu(x, -\bar{\zeta}) dx \\ &= \int_{\Omega} e^{-iy \cdot \xi} q(y) \overline{\mu(y, \bar{\zeta})} dy \\ &= \mathbf{t}(\xi, \bar{\zeta}). \end{aligned}$$

□

We now have a corollary for spherically symmetric potentials:

Corollary 3.3. *Suppose q is spherically symmetric. Then*

$$\overline{\mathbf{t}(\xi, \zeta)} = \mathbf{t}(\xi, \zeta), \quad \xi \in \mathbf{R}^3, \zeta \in \mathcal{V}_\xi.$$

Proof. There exists $R \in SO(2)$ such that

$$R(\xi) = \xi, \quad R(\zeta) = \bar{\zeta},$$

and hence from (24) we have $\mathbf{t}(\xi, \zeta) = \mathbf{t}(\xi, \bar{\zeta})$. Equation (26) now implies the result for \mathbf{t} . For \mathbf{t}^{exp} the result follows similarly. □

3.2. Eigenfunctions and eigenvalues for the Dirichlet-to-Neumann map

We use the same ideas for the computation of eigenvalues for the 3-D problem that were used for the 2-D problem in [SMI00].

Proposition 3.4. *Let D be the unit disk and suppose $\gamma(x)$ is spherically symmetric. Then the eigenfunctions of Λ_γ are the spherical harmonics Y_l^m .*

Proof. When γ is spherically symmetric it follows from separation of variables that the solution to $\nabla \cdot \gamma \nabla u_{lm} = 0$ with $u_{lm}|_{\partial D} = Y_l^m$ is

$$u_{lm} = R_l(r) Y_l^m(\theta, \phi), \quad (27)$$

where $R_l(r)$ solves an Euler type equation. Thus

$$\Lambda_\gamma Y_l^m(\theta, \phi) = \Lambda_\gamma u|_{r=1} = \gamma \frac{\partial R_l}{\partial r} \Big|_{r=1} Y_l^m(\theta, \phi) = \lambda_l Y_l^m(\theta, \phi). \quad (28)$$

□

Note that λ is independent of m since R_l is independent of m .

3.3. Approximation of Eigenvalues and Eigenfunctions of the Dirichlet-to-Neumann Map

Next we will consider how to approximate the eigenvalues for the special case of a constant conductivity $\gamma = 1$. The particular form of R_l gives the following result.

Proposition 3.5. *The eigenvalues of Λ_1 are given by $\lambda_l = l$.*

In the case of a piecewise constant radially symmetric conductivity the eigenvalues can be computed recursively. Suppose $0 = r_0 < r_1 < r_2 < \dots < r_{N-1} < r_N = 1$ and for $j = 1, 2, \dots, N$

$$\gamma(x) = \gamma_j > 0, \quad |x| \in [r_{j-1}, r_j]. \quad (29)$$

Proposition 3.6. *Suppose γ is given by (29). Then the eigenvalues of Λ_γ are given by*

$$\lambda_0 = 0, \quad \lambda_l = l - \frac{2l+1}{1+C_{N-1}}, \quad l > 0$$

where $C_j = w_j \frac{\beta_l \gamma_{j+1} \rho_j + \gamma_j}{\gamma_{j+1} \rho_j - \gamma_j}$ with $\rho_1 = 1$, $\rho_j = \frac{C_{j-1} + w_j}{C_{j-1} - \beta_l w_j}$, $\beta_l = \frac{l+1}{l}$ and $w_j = r_j^{-(2l+1)}$.

Proof. Since Y_0^0 is a constant, $\lambda_0 = 0$. The solution to $\nabla \cdot \gamma \nabla u_{lm} = 0$, $u_{lm}|_{\partial D} = Y_l^m$, is given by (27) with $R_l(r) = A_j r^l + B_j r^{-(l+1)}$ for $r_{j-1} \leq r < r_j$, $j = 1, \dots, N$. The coefficients A_j and B_j are determined by matching the Dirichlet and Neumann conditions at the r_j , $j = 1, \dots, N-1$. The outermost Dirichlet condition (at $r = 1$) gives $1 = A_N + B_N$ which leads to the following eigenvalue expression:

$$\lambda_l = \gamma \left. \frac{\partial v_{lm}}{\partial r} \right|_{\partial D} = l A_N - (l+1) B_N = l - (2l+1) B_N \quad (30)$$

Moreover, by induction it follows that $A_j = B_j C_{j-1}$ for $j = 2, \dots, N$. Again using the Dirichlet condition from the boundary, $1 = A_N + B_N$ we get $B_N = (C_{N-1} + 1)^{-1}$ which leads to the expression of the eigenvalue as stated in the theorem. \square

By [SCII91] if conductivities γ_L and γ_U are such that $\gamma_L(r) \leq \gamma_U(r)$ for all r , then the eigenvalues λ_l^L and λ_l^U of their corresponding Dirichlet-to-Neumann maps satisfy $\lambda_l^L \leq \lambda_l^U$. This gives a means for finding lower and upper bounds on the eigenvalues of a smooth function by finding the eigenvalues of piecewise constant function, γ_L and γ_U that satisfy $\gamma_L(r) \leq \gamma(r) \leq \gamma_U(r)$.

4. Implementation details

4.1. Numerical method for computing the scattering transform $\mathbf{t}(\xi, \zeta)$

We compute the scattering transform $\mathbf{t}(\xi, \zeta)$ from the definition (13) as a comparison to the \mathbf{t}^{exp} approximation and to study the reconstructions from an accurate scattering transform. The computation requires that we solve the Lippmann-Schwinger equation (12) for $\mu(x, \zeta)$. Hence we require

- A method of computation for the Faddeev Green's function in three dimensions

- A numerical method for the solution of (12)
- Numerical quadrature for computing $\mathbf{t}(\xi, \zeta)$ from (13)

We describe each of these in turn.

4.1.1. Computation of the Faddeev Green's function The Faddeev Green's function was defined in equations (10). The effect of scaling and rotation of ζ on G_ζ was analyzed in [CKS06], and it was shown that when ζ satisfying $\zeta \cdot \zeta = 0$ is decomposed in the form

$$\zeta = \kappa(k_\perp + ik), \quad (31)$$

where $k_\perp, k \in \mathbf{R}^3$, $|k_\perp| = |k| = 1$, $k \cdot k_\perp = 0$, and $|\zeta| = \sqrt{2}\kappa$, then

$$g_\zeta(x) = \kappa^{n-2} g_{k_\perp + ik}(\kappa x). \quad (32)$$

Furthermore, if $R \in SO(2)$ then

$$g_\zeta(x) = g_{\mathbf{R}\zeta}(Rx). \quad (33)$$

Combining (32) and (33) yields the formula

$$g_\zeta(x) = \kappa g_{e_1 + ie_2}(\kappa Rx), \quad (34)$$

where $R \in SO(2)$ and the first and second column of R is k, k_\perp respectively. This formula shows that it is sufficient to compute $g_{e_1 + ie_2}$.

To compute $g_{e_1 + ie_2}$ we will use formula (6.4) of [New89]

$$g_{e_1 + ie_2}(x) = \frac{e^{-r+x_2-ix_1}}{4\pi r} - \frac{1}{4\pi} \int_s^1 \frac{e^{-ru+x_2-ix_1}}{\sqrt{1-u^2}} J_1(r\sqrt{1-u^2}) du, \quad (35)$$

where J_1 denotes the Bessel function of the first kind of order one. Here $r = |x|$ and $s = \hat{x} \cdot e_2 = x/|x| \cdot e_2$. Since the function $J_1(t)/t$ is continuous on the interval $[0, \infty)$ (in particular at $t = 0$), we will approximate the integral in (35) by a simple midpoint Riemann sum

$$\int_s^1 \frac{e^{-ru+x_2-ix_1}}{\sqrt{1-u^2}} J_1(r\sqrt{1-u^2}) du \approx \sum_{j=1}^N \frac{e^{-ru(j)+x_2-ix_1}}{\sqrt{1-u(j)^2}} J_1(r\sqrt{1-u(j)^2}) h,$$

where N is the number of discretization points, $h = (1-s)/N$ and $u(j) = s + (j-1/2)h$, $j = 1, 2, \dots, N$.

4.1.2. The computation of complex geometrical optics Having computed the Faddeev Green's function we now turn to the numerical solution of the integral equation (12) for $\mu(\cdot, \zeta)$. We will use a method due to Vainikko [Vai00] for solving Lippmann-Schwinger equations; see also [Hoh01, KMS04] for implementations in different contexts. The main idea is to transform (12) to a multiperiodic integral equation in \mathbf{R}^3 , which can be solved efficiently using FFT.

Let $G_\rho = \{x \in \mathbf{R}^3 \mid |x_i| \leq \rho\}$. Then by assumption $\text{supp}(q) \subset \Omega \subset G_1$. Extend the potential q and the Green's function g_ζ to G_2 such that

$$q^p(x) = \begin{cases} q(x), & x \in \Omega, \\ 0, & x \in G_2 \setminus \Omega, \end{cases} \quad g_\zeta^p(x) = \begin{cases} g_\zeta(x), & x \in \Omega, \\ 0, & x \in G_2 \setminus \Omega, \end{cases}$$

and then extend q^p and g_ζ^p to \mathbf{R}^3 as periodic functions in all variables with period equal to 4. Instead of (12) we consider the periodic integral equation

$$\mu^p(x, \zeta) + \int_{\mathbf{R}^3} g_\zeta^p(x - y) q^p(y) \mu^p(y, \zeta) dy = 1. \quad (36)$$

This equation is uniquely solvable since (12) is, and moreover one can show that on Ω we have

$$\mu^p(x, \zeta) = \mu(x, \zeta), \quad x \in \Omega.$$

In order to solve (36) numerically define

$$\mathbb{Z}_N^3 = \{j \in \mathbb{Z}^3 \mid -N/2 \leq j_k < N/2, k = 1, \dots, 3\}$$

and the computational grid

$$C_N = h\mathbb{Z}_N^3$$

where $h = 4/N$ specifies the discretization fineness. Define the grid approximation ϕ_N of a continuous function $\phi \in C(G_2)$ by

$$\phi_N(jh) = \phi(jh)$$

and the grid approximation g_N of g_ζ^p (which is smooth except for a singularity at the origin) for fixed ζ by

$$g_N(jh) = \begin{cases} 0, & j = 0 \\ g_\zeta^p(jh), & \text{otherwise.} \end{cases}$$

The convolution operator appearing in (36)

$$K\phi(x) = \int_{\mathbf{R}^3} g_\zeta^p(x - y) \phi(y) dy$$

is now discretized by trigonometric collocation, which, using the discrete Fourier transform \mathcal{F}_N , gives

$$K_N \phi_N(jh) = \mathcal{F}_N^{-1}(\hat{g}_N^p \cdot \hat{\phi}_N).$$

Here \cdot denotes pointwise multiplication. In practice the discrete Fourier transform can be implemented efficiently using FFT (with proper zero-padding) in $\mathcal{O}(N^3 \log(N))$ arithmetic operations. The total discretization of (36) now reads

$$\mu_N + K_N(q_N \mu_N) = Q_N 1.$$

This discrete linear system is solved numerically in matlab using the iterative algorithm GMRES [SS86], without setting up a matrix for the linear map $K_N(q_N \cdot)$.

4.1.3. The scattering transform Having computed the grid approximation μ_N it is straightforward to evaluate $t(\xi, \zeta)$ by using numerical integration in (13). In this implementation we have used a simple midpoint quadrature rule.

4.2. Numerical method for computing \mathbf{t}^{exp} for spherically symmetric conductivities

For the calculation of \mathbf{t}^{exp} we expand $e^{ix \cdot \zeta}$ in terms of spherical harmonics[‡] and $e^{-ix \cdot (\xi + \zeta)}$ in terms of the spherical harmonics conjugates,

$$\begin{aligned} e^{-ix \cdot (\xi + \zeta)} &= \sum_{l=0}^{\infty} \sum_{m=-l}^l a_{lm}^*(\xi, \zeta) [Y_l^m(\theta, \phi)]^* \\ e^{ix \cdot \zeta} &= \sum_{k=0}^{\infty} \sum_{n=-k}^k b_{kn}(\zeta) Y_k^n(\theta, \phi). \end{aligned}$$

Using these expansions leads to

$$\mathbf{t}^{\text{exp}}(\xi, \zeta) = \sum_{l,m} \sum_{k,n} a_{lm}^*(\xi, \zeta) b_{kn}(\zeta) \int_{\partial D} [Y_l^m(\theta, \phi)]^* (\Lambda_q - \Lambda_0) Y_k^n(\theta, \phi) d\sigma \quad (37)$$

In the special case of spherically symmetric conductivities we can use the knowledge of the eigenvalues of the Dirichlet-to-Neumann maps, $\Lambda_\gamma Y_l^m(\theta, \phi) = \lambda_l Y_l^m$ to simplify the calculation of \mathbf{t}^{exp} . In particular we get

$$\begin{aligned} \mathbf{t}^{\text{exp}}(\xi, \zeta) &= \sum_{l,m,k,n} a_{lm}^*(\xi, \zeta) b_{kn}(\zeta) \int_{\partial D} [Y_l^m(\theta, \phi)]^* (\lambda_k - k) Y_k^n(\theta, \phi) d\sigma \\ &= \sum_{l,m,k,n} a_{lm}^*(\xi, \zeta) b_{kn}(\zeta) (\lambda_k - k) \int_{\partial D} [Y_l^m(\theta, \phi)]^* Y_k^n(\theta, \phi) d\sigma \\ &= \sum_{l,m} a_{lm}^*(\xi, \zeta) b_{lm}(\zeta) (\lambda_l - l) \end{aligned} \quad (38)$$

The last equality comes from the orthonormality of the spherical harmonics. Equation (38) can be easily calculated if the coefficients a_{lm}^* and b_{lm} are available. In this work, these coefficients were calculated with a software package called ‘*S2kit*’ which are C routines that can be accessed from Matlab. Detailed information can be found in [HRKM03].

4.3. Computation of the conductivity

After taking the high frequency limit in (16) and (18) we calculate the inverse Fourier transform to get $q(x)$ and $q^{\text{exp}}(x)$. The integral in the inverse Fourier transform is here computed numerically using a simple Riemann sum. To get the conductivity γ we need to solve the boundary value problem $\Delta \gamma^{1/2} = q \gamma^{1/2}$ with $\gamma^{1/2}|_{\partial \Omega} = 1$. This was realized with the standard Green’s function for the Laplace equation in three dimensions. Using symmetries reduces the problem to a single integral.

4.4. Numerical implementation of Calderón’s method

Calderón’s method based on (23) is simply implemented by evaluating the integral using numerical quadrature.

[‡] We use here the normalized spherical harmonics given by $Y_l^m(\theta, \phi) = N_l^m P_l^m(\cos \theta) e^{im\phi}$ where N_l^m are normalization factors and P_l^m are associated Legendre functions.

5. Results

5.1. Examples

The conductivity distributions we will use in the examples are smooth, spherically symmetric and constant one near $\partial\Omega$. They are given by

$$\begin{aligned} \gamma(x) &= (\alpha\Psi(|x|) + 1)^2 \\ \Psi(r) &= \begin{cases} e^{-\frac{r^2}{(r^2-d^2)^2}} & \text{for } -d < r < d \\ 0 & \text{otherwise} \end{cases} \end{aligned} \quad (39)$$

where $0 < d \leq 1$ is a parameter determining the support of Ψ . The parameter α regulates the amplitude of γ , which is largest at $r = 0$ with amplitude $(\alpha + 1)^2$. A similar function was used [SMI00] as an example for the two dimensional problem.

5.2. The scattering transform

Let us fix $d = 0.9, \alpha = 0.3$ in (39). We are interested in the limit of $\mathbf{t}(\xi, \zeta), \xi \in \mathbf{R}^3, \zeta \in \mathcal{V}_\xi$, when $|\zeta|$ goes to infinity. For purpose of illustration we compute $\mathbf{t}(\xi, \zeta)$ for fixed $\xi = (10, 0, 0)$ and varying $\zeta \in \mathcal{V}_\xi$ with $8 < |\zeta| < 50$. We use a discretization level in the algorithm corresponding to $N = 2^6$. In addition we compute $\mathbf{t}^{\text{exp}}(\xi, \zeta)$ by (37) using the first 30 eigenvalues of the Dirichlet-to-Neumann map. We truncate the sum of the spherical harmonics at $l = 30$, which means we use approximately the first 900 spherical harmonics. As a benchmark we compute $\hat{q}(\xi)$. The results are shown in figure 1. We know from Corollary 3.3 that \mathbf{t} and \mathbf{t}^{exp} are real and this is consistent with our

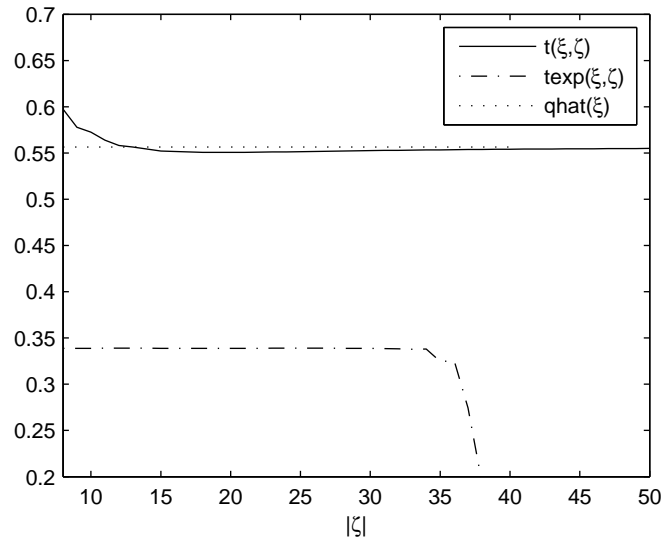


Figure 1. $\mathbf{t}(\xi, \zeta), \mathbf{t}^{\text{exp}}(\xi, \zeta)$ calculated for fixed $\xi = (10, 0, 0)$ and varying $|\zeta|$. Here $d = 0.9$ and $\alpha = 0.3$.

numerical results. The data verifies that for our example $\mathbf{t}(\xi, \zeta)$ converges to $\hat{q}(\xi)$ as $\zeta \rightarrow \infty$. We observe that \mathbf{t}^{exp} is independent of the magnitude of $\zeta \in \mathcal{V}_\xi$, until it diverges

due to numerical instability. The same phenomena appears in other examples and with different values of ξ . We believe that this phenomena has to do with the special class of spherically symmetric conductivities considered here.

Next we compare $\mathbf{t}(\xi, \zeta)$ and $\mathbf{t}^{\text{exp}}(\xi, \zeta)$ for different values of ξ . For each $\xi = s[1, 0, 0]$, $s \in [0, 50]$, we fix $\zeta \in \mathcal{V}_\xi$ with $|\zeta| = 50$. We compute $\mathbf{t}(\xi, \zeta)$ using a discretization level with $N = 2^6$. \mathbf{t}^{exp} is computed with the parameters as above. As a benchmark we compute $\hat{q}(\xi)$. The results are displayed in figure 2. The difference in $\hat{q}(\xi)$

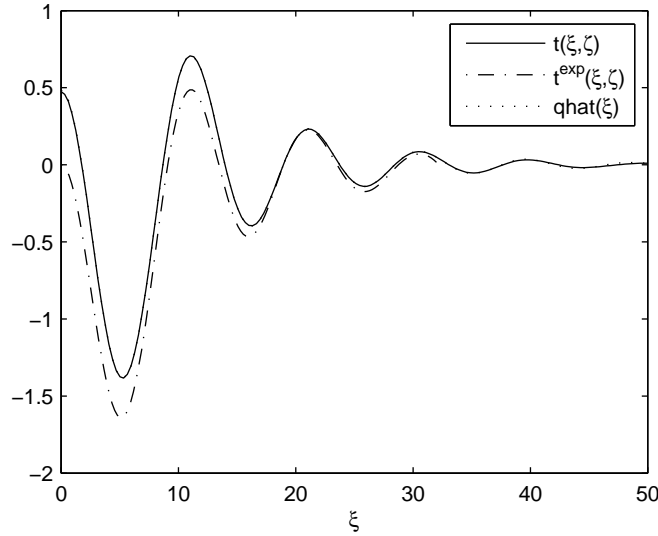


Figure 2. Scattering data \mathbf{t} , \mathbf{t}^{exp} and \hat{q} (qhat) with $d = 0.9$ and $\alpha = 0.3$. For each ξ , $\zeta \in \mathcal{V}_\xi$ is chosen such $|\zeta| = 50$. The Fourier transform \hat{q} virtually coincides with $\mathbf{t}(\xi, \zeta)$.

and $\mathbf{t}(\xi, \zeta)$ is very small. $\mathbf{t}^{\text{exp}}(\xi)$ is displayed only for $0 \leq |\xi| \leq 32$ since the calculation becomes numerically unstable and blows up for $|\xi| > 32$. One observes good agreement of all three curves for $|\xi| \geq 20$. Close to $|\xi| = 0$ the approximation \mathbf{t}^{exp} is close to zero and differs from the correct values.

5.3. The reconstructions

Evaluating the inverse Fourier transform of the numerically computed $\mathbf{t}^{\text{exp}}(\xi)$ and $\mathbf{t}(\xi, \zeta)$ gives two approximations of $q(x)$ which are displayed in figure 3. The approximation calculated from $\mathbf{t}(\xi, \zeta)$ differs as expected only slightly from the actual value. The approximation q^{exp} of q calculated from \mathbf{t}^{exp} (and hence from the boundary data) is quite different from q . For x near the boundary the $q^{\text{exp}}(x)$ is quite accurate, but for x near zero there are large discrepancies, especially in the magnitude. Looking at the scattering data in figure 2, one sees two features most likely responsible for that difference. The first one is the differences in the values of $\mathbf{t}^{\text{exp}}(\xi)$ for ξ close to zero compared to $\hat{q}(\xi)$. The second is the truncation of $\mathbf{t}^{\text{exp}}(\xi)$ due to numerical instability for large ξ values. More details on the influence of the truncation of the scattering data are provided in section 5.4.

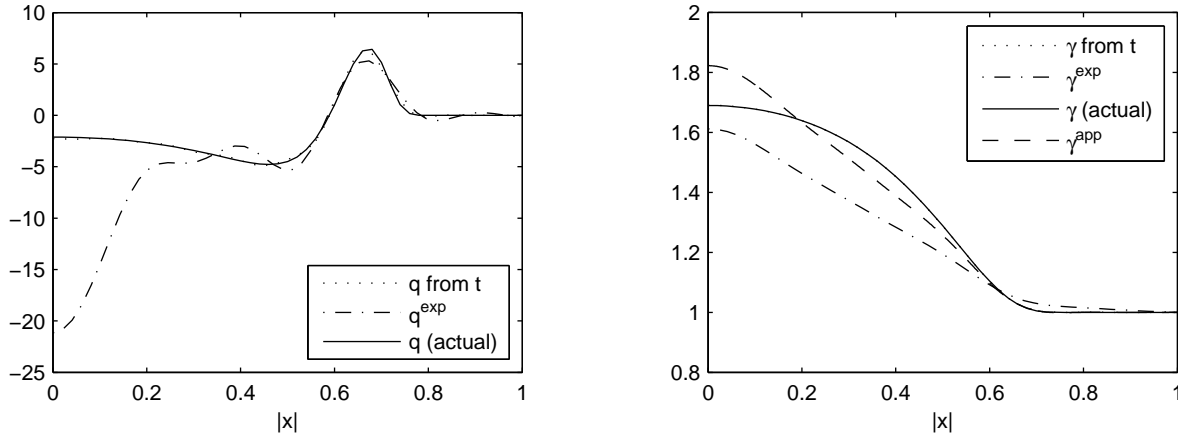


Figure 3. Left: Reconstructions of $q(x)$ by taking the inverse Fourier transform of $\mathbf{t}(\xi, \zeta)$ and $\mathbf{t}^{\text{exp}}(\xi, \zeta)$ for $\alpha = 0.3$ and $d = 0.9$. Right: Reconstructions of γ from \mathbf{t} , γ^{exp} , and γ^{app} compared to actual conductivity for $\alpha = 0.3$ and $d = 0.9$. γ from \mathbf{t} nearly coincides with the actual conductivity.

Also in figure 3 we display three reconstructions of the conductivity distribution. The first reconstruction of γ is from $\mathbf{t}(\xi, \zeta)$. Since $\mathbf{t}(\xi, \zeta)$ is computed from the forward problem, it may be expected that this reconstruction would be very close to the actual value, as it is. The second reconstruction is $\gamma^{\text{exp}}(x)$ from \mathbf{t}^{exp} , and the third reconstruction γ^{app} is from the linear method (23). Considering the relatively large difference in magnitude of $q^{\text{exp}}(x)$, the reconstruction γ^{exp} is surprisingly good. Also γ^{app} is a fairly good reconstruction. A positive aspect in both reconstructions is that we get $\gamma \equiv 1$ close to the boundary. Moreover, the overall shape is also fairly well reconstructed.

5.4. The influence of the truncation of the scattering data

When we reconstructed q^{exp} and γ^{exp} we truncated the scattering data \mathbf{t}^{exp} due to numerical instabilities. In this section we investigate the influence on the reconstructions of the truncation of the true scattering data $\mathbf{t}(\xi, \zeta)$. Figure 4 shows $\mathbf{t}(\xi, \zeta)$ and the reconstructions $q(x)$ and $\gamma(x)$ for different truncations of $\mathbf{t}(\xi, \zeta)$, namely at $\xi = R$ for $R = 15, 25, 50$. We have chosen $\zeta \in \mathcal{V}_\xi$ with $|\zeta| = 50$. The actual potential and conductivity are almost identical to the curves corresponding to $R = 50$. It is evident that the amount of truncation of the scattering transform influences the reconstruction, and that a very poorly reconstructed q can still result in a good approximation of γ . This suggests that for the reconstruction of γ the values of the scattering data for small ξ are very important. This is analogous to observations made in the 2-D case [MS03].

5.5. Influence of the support and magnitude of $\gamma(x)^{1/2} - 1$

So far we have used fixed values for d and α , which determine the support and the magnitude of $\gamma(x)^{1/2} - 1$. Figure 5 displays the reconstructions γ^{exp} and γ^{app} of $\gamma(x)$

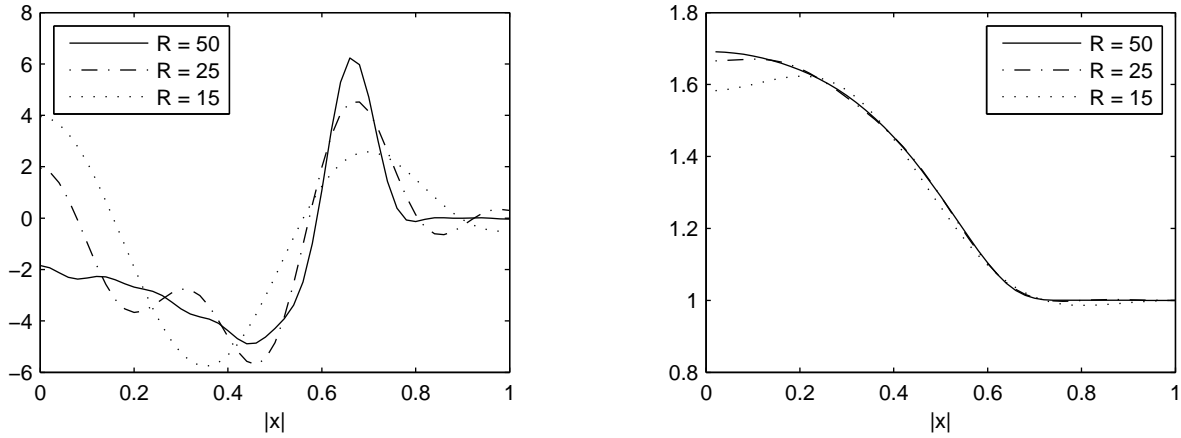


Figure 4. Left: reconstructed Schrödinger potential with truncation of \mathbf{t} at $R = 15, 25$, and 50. Right: reconstructions of γ .

from $\mathbf{t}^{\text{exp}}(\xi)$ for different choices of support d and magnitude α . Each row corresponds to a certain d -value and each column to a specific α -value. For small support and small magnitude we get good reconstructions, but the quality changes dramatically with larger amplitude and larger support. Especially γ^{exp} does not recover the actual conductivity very well for the large amplitude $\alpha = 0.9$.

6. Conclusions

In this work a direct method based on [Nac88] for reconstructing a 3-D conductivity distribution from the Dirichlet-to-Neumann map was implemented and tested on noise-free data. A linearizing approximation to the scattering transform, denoted \mathbf{t}^{exp} was studied and compared to Calderón’s reconstruction algorithm. Reconstructions of spherically symmetric conductivities in the unit sphere were computed using the \mathbf{t}^{exp} approximation, Calderón’s method, and a scattering transform computed from the definition requiring knowledge of the actual Schrödinger potential. The latter case served as a benchmark to study the quality of reconstructions for which the actual scattering transform is known. It was shown that very accurate reconstructions can be obtained from accurate knowledge of the scattering transform. It was found that in contrast to the 2-D case, the \mathbf{t}^{exp} approximation is inaccurate near the origin, and this results in poor approximations to the magnitude of the conductivity. However, the support of $\gamma - 1$ and the boundary value $\gamma = 1$ was well approximated by all three methods. Truncating the computed scattering transform in the computations was found to have a profound effect on the reconstructed Schrödinger potential q , but the affect on the reconstructed conductivity γ was less dramatic. In summary, it appears that the use of the full scattering transform in this method is a promising approach for 3-D reconstructions, while linearizations lead to significant inaccuracies in the reconstructed amplitudes.

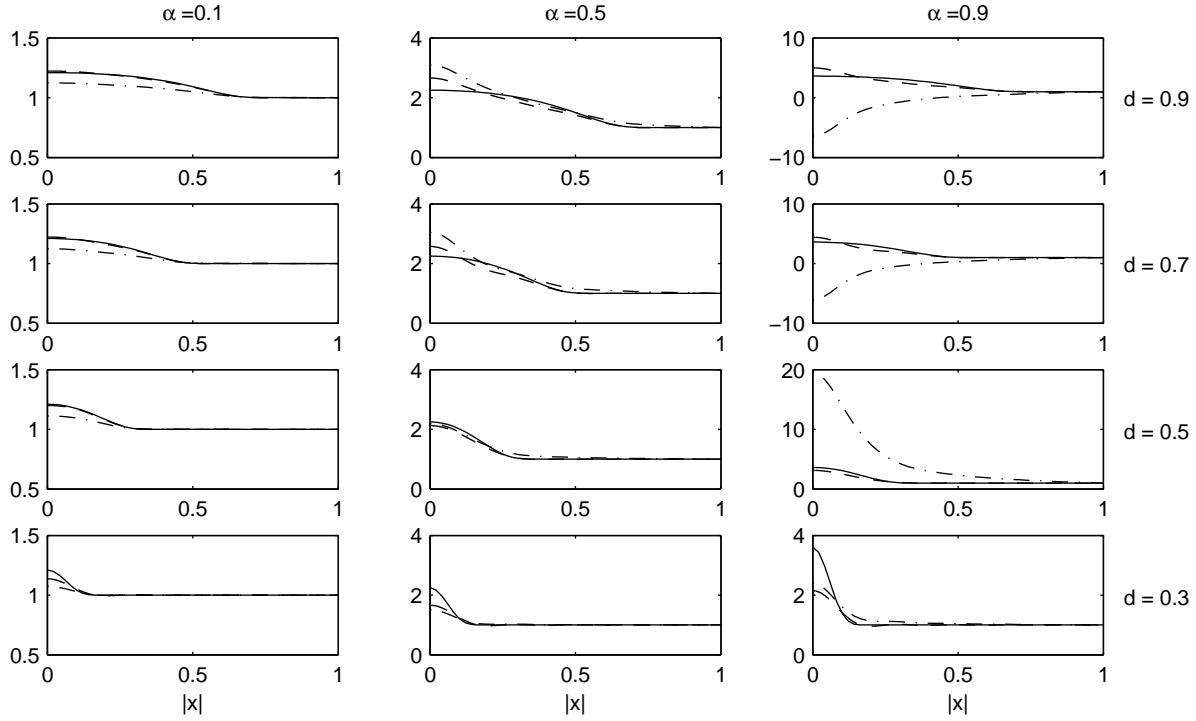


Figure 5. Reconstructions of conductivities of varying support and magnitude: each row corresponds to a specific support d and each column corresponds to a specific magnitude of γ . The dash-dotted curves are the γ^{exp} reconstructions, the dashed curves are the γ^{app} reconstructions, and solid curves are the actual conductivities γ .

Acknowledgments

The authors thank D. Isaacson and G. Boverman for helpful discussions on the spherical harmonics. This material is based upon work supported by the National Science Foundation under Grant No. 0513509 (J. Mueller).

References

- [AP06a] K. Astala and L. Päivärinta, *A boundary integral equation for Calderón's inverse conductivity problem*, Collect. Math. (2006), no. Vol. Extra, 127–139.
- [AP06b] K. Astala and L. Päivärinta, *Calderón's inverse conductivity problem in the plane*, Ann. of Math. (2) **163** (2006), no. 1, 265–299.
- [BM08] J. Bikowski and J. Mueller, *2D EIT reconstructions using Calderón's method*, Inverse Probl. Imaging, **2** (2008), no. 1, 43–61.
- [BTJIS08] G. Boverman, K. Tzu-Jen, D. Isaacson, and G. Saulnier, *An implementation of calderón's method for 3-d limited view eit*, IEEE Trans. Med. Imaging **1** (2008), no. 1, 1–10.
- [BT03] R. Brown and R. H. Torres, *Uniqueness in the inverse conductivity problem for conductivities with 3/2 derivatives in L^p , $p > 2n$* , J. Fourier Anal. Appl. **9** (2003), no. 6, 563–574.
- [BU97] R. Brown and G. Uhlmann, *Uniqueness in the inverse conductivity problem for nonsmooth*

- conductivities in two dimensions*, Comm. Partial Differential Equations **22** (1997), no. 5-6, 1009–1027.
- [Cal80] A. Calderón, *On an inverse boundary value problem*, Seminar on Numerical Analysis and its Applications to Continuum Physics (Rio de Janeiro, 1980), Soc. Brasil. Mat., Rio de Janeiro, 1980, pp. 65–73.
- [CKS06] H. Cornean, K. Knudsen, and S. Siltanen, *Towards a d-bar reconstruction method for three-dimensional EIT*, J. Inverse Ill-Posed Probl. **14** (2006), no. 2, 111–134.
- [DM10] M. DeAngelo and J. Mueller, *D-bar reconstructions of human chest and tank data using an improved approximation to the scattering transform*, Physiol. Meas. **31** (2010), no. 2, 221–232.
- [Hoh01] T. Hohage, *On a numerical solution of a three-dimensional inverse medium scattering problem*, Inverse Problems **17** (2001), no. 6, 1743–1763.
- [HRKM03] D. Healy, Jr., D. Rockmore, P. Kostelec, and S. Moore, *FFTs for the 2-sphere-improvements and variations*, J. Fourier Anal. Appl. **9** (2003), no. 4, 341–385.
- [Hol05] D. Holder *Electrical impedance tomography*. first edition, Institute of Physics Publishing, Bristol and Philadelphia, 2005.
- [IMNS04] D. Isaacson, J. Mueller, J. Newell, and S. Siltanen. Reconstructions of chest phantoms by the d-bar method for electrical impedance tomography. *IEEE Trans Med Imaging*, **23** (2004), no 7, 821–828.
- [IMNS06] D. Isaacson, J. Mueller, J. Newell, and S. Siltanen. Imaging cardiac activity by the d-bar method for electrical impedance tomography. *Physiol. Meas.*, **27**, 2006.
- [Knu03] K. Knudsen *A new direct method for reconstructing isotropic conductivities in the plane*, Physiological Measurements, **24** (2003), no. 2, 391–401.
- [KLMS07] K. Knudsen, M. Lassas, J. Mueller, and S. Siltanen, *D-bar method for electrical impedance tomography with discontinuous conductivities*, SIAM J. Appl. Math., **67** (2007), no. 3, 893–913.
- [KLMS09] K. Knudsen, M. Lassas, J. Mueller, and S. Siltanen, *Regularized D-bar method for the inverse conductivity problem*, Inverse Probl. Imaging, **3** (2009), no 4, 599–624.
- [KMS04] K. Knudsen, J. Mueller, and S. Siltanen, *Numerical solution method of the dbar-equation in the plane*, Journal of Computational Physics **198** (2004), no. 2, 500–517.
- [KT04] K. Knudsen and A. Tamasan, *Reconstruction of less regular conductivities in the plane*, Comm. Partial Differential Equations **29** (2004), no. 3-4, 361–381.
- [MS03] J. Mueller and S. Siltanen, *Direct reconstruction of conductivities from boundary measurements*, Siam J. Sci. Comp. **24** (2003), no. 4, 1232–1266.
- [EM09] E. Murphy and J. Mueller, *Effect of errors in domain shape modeling in 2-D reconstructions by the D-bar method*, IEEE Trans. Med. Imaging **28** (2009), no. 10, 1576–1584.
- [Nac88] A. Nachman, *Reconstructions from boundary measurements*, Ann. of Math. (2) **128** (1988), no. 3, 531–576.
- [Nac96] A. Nachman, *Global uniqueness for a two-dimensional inverse boundary value problem*, Ann. of Math. (2) **143** (1996), no. 1, 71–96. MR 96k:35189
- [New89] R. Newton, *Inverse Schrödinger scattering in three dimensions*, Springer-Verlag, Berlin, 1989.
- [Nov88] R. Novikov, *A multidimensional inverse spectral problem for the equation $-\Delta\psi + (v(x) - Eu(x))\psi = 0$* , Funktsional. Anal. i Prilozhen. **22** (1988), no. 4, 11–22, 96, translation in Funct. Anal. Appl., **22** (1988), no. 4, 263–272.
- [NSU88] A. Nachman, J. Sylvester, and G. Uhlmann, *An n -dimensional Borg-Levinson theorem*, Comm. Math. Phys. **115** (1988), no. 4, 595–605.
- [PPU03] L. Päivärinta, A. Panchenko, and G. Uhlmann, *Complex geometrical optics solutions for Lipschitz conductivities*, Rev. Mat. Iberoamericana **19** (2003), no. 1, 56–72.
- [SCII91] E. Somersalo, M. Cheney, D. Isaacson, and E. Isaacson, *Layer stripping: a direct numerical method for impedance imaging*, Inverse Problems **7** (1991), no. 6, 899–926.

- [SMI00] S. Siltanen, J. Mueller, and D. Isaacson, *An implementation of the reconstruction algorithm of A. Nachman for the 2D inverse conductivity problem*, Inverse Problems **16** (2000), no. 3, 681–699. Erratum in Inverse Problems **17** (2001), no. 5, 1561–1563.
- [SMI01] S. Siltanen, J. Mueller, and, D. Isaacson, *Reconstruction of high contrast 2-D conductivities by the algorithm of A. Nachman*, in Radon transforms and tomography (South Hadley, MA, 2000), 241–254, Contemp. Math., 278, Amer. Math. Soc., Providence, RI, 2001.
- [SS86] Y. Saad and M. Schultz, *GMRES: a generalized minimal residual algorithm for solving nonsymmetric linear systems*, SIAM J. Sci. Statist. Comput. **7** (1986), no. 3, 856–869.
- [SU87] J. Sylvester and G. Uhlmann, *A global uniqueness theorem for an inverse boundary value problem*, Ann. of Math. (2) **125** (1987), no. 1, 153–169.
- [Vai00] G. Vainikko, *Fast solvers of the Lippmann-Schwinger equation*, Direct and inverse problems of mathematical physics (Newark, DE, 1997), Kluwer Acad. Publ., Dordrecht, 2000, pp. 423–440.